Journal of Materials Chemistry A

Accepted Manuscript

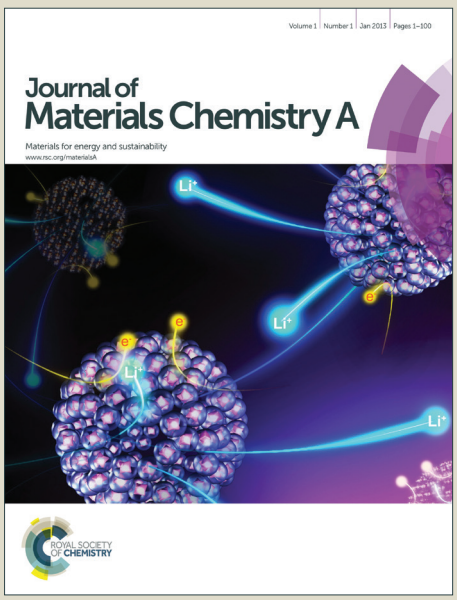

ROYAL SOCIETY OF CHEMISTRY

www.rsc.org/materialsA

Journal Name

RSCPublishing

ARTICLE

Enhanced microwave absorption of ZnO coated with Ni nanoparticles produced by atomic layer deposition

Cite this: DOI: 10.1039/xoxxoooooox

Guizhen Wang,[a] Xiange Peng,[a] Lei Yu,[a] Gengping Wan,*[a] Shiwei Lin*[a] and Yong Qin*[b]

Received ooth January 2012,
Accepted ooth January 2012

DOI: 10.1039/xoxxoooooox

www.rsc.org/

In this work, the flower-like ZnO coated by Ni nanoparticles has been synthesized by the reduction of NiO-coated ZnO produced by an atomic layer deposition (ALD) method. The structure and electromagnetic (EM) absorption properties of the as-prepared samples are investigated. By applying 800 ALD cycles of NiO deposition followed by a reduction process, the surfaces of ZnO are densely covered by Ni nanoparticles with a narrow particle size distribution and an average size of 13.1 nm. The ZnO@Ni exhibit remarkably improved EM absorption properties compared to the ZnO. The optimal RL calculated from the measured complex permittivity and permeability is −48.0 dB at 10.4 GHz. Moreover, the EM wave absorption less than −10 dB is found to reach 5.3 GHz for an absorber thickness of 1.5 mm. The enhanced absorption ability arises from the effective combination of multiple dielectric−magnetic loss mechanisms.

1. Introduction

In recent years, many investigations have been concentrated on the microwave absorbing materials (MAMs) for increasing electromagnetic (EM) interference problems which are discharged from the wide use of communication devices in the gigahertz (GHz) band range. Numerous candidates, including dielectric absorbers such as carbonaceous material,[1–4] ceramics,[5,6] conducting polymers[7,8] and magnetic materials such as magnetic metallic fillers,[9,10] ferrites[11,12] and intermetallic compounds[13] have been developed to meet versatile application requirements. Recently, it has been confirmed that ZnO can also be used as a major annexing agent of microwave absorbers due to its lightweight, semiconductive, and piezoelectric features.[14–17] For example, Zhuo *et al.*[18] synthesized the hierarchical ZnO nanotrees via a two-step chemical vapor deposition process and found that the optimal absorption for the ZnO nanotrees was −58 dB at 4.2 GHz with a thickness of 4.0 mm. They considered that excellent absorption was attributed to the isotropic antenna shape of ZnO nanotrees. Zhang et al.[19] reported the synthesis of crossed ZnO netlike structures through the direct evaporation of metal zinc and graphite powders without any catalyst. Their results showed that the ZnO netlike structures/paraffin composites also present the high performance of microwave absorption. Despite tremendous research efforts, enhancing the absorbing capacity of ZnO still remains a challenge for large scale use.

To obtain improved EM wave absorption performance, absorbing materials need to have a suitable dielectric loss and magnetic loss, namely efficient EM impedance matching between the relative permittivity and permeability. ZnO is nonmagnetic and thus its electromagnetic absorption properties mostly derive from dielectric loss. For achieving strong absorption and broad bandwidth, one of the effective ways to solve the problem is to integrate ZnO with magnetic materials.[20] Especially, it has been reported that many core−shell structured composites show better microwave absorption performance than the pure core or shell materials.[21–25] However, as an amphoteric oxide, ZnO has less resistance to acid and alkali. Thus it is still difficult to realize dielectric−magnetic coupled ZnO-based absorption materials using the traditional solution methods.

In this study, we employed an atomic layer deposition (ALD) technology to fabricate the interesting Ni-coated ZnO (ZnO@Ni) core−shell composites and investigated their microwave absorption properties. Benefiting from the uniform coatings of Ni nanoparticles, the interfacial polarization, dielectric properties and magnetic loss of ZnO@Ni are greatly enhanced, which lead to remarkably improved microwave absorption properties compared to ZnO.

2. Experimental

2.1 Preparation of ZnO

20 mL of 20 mmol·L^{-1} zinc acetate aqueous solution was mixed with a NaOH aqueous solution (0.3 mol·L^{-1}) of the same volume under vigorous magnetic stirring at room temperature. The mixture solution was then transferred into a 50 mL Teflon-

lined stainless steel autoclave and was kept at 160 °C for 5 h. The resultant white solid product was centrifuged, washed with distilled water, and dried at 45 °C in a vacuum.

2.2 Synthesis of ZnO@Ni

The ALD process was carried out in a home-made, closed type, hot-wall ALD reactor. Prior to ALD, the ZnO was dispersed in ethanol by ultrasonic agitation and then dropped onto a quartz wafer. After being air-dried, the NiO coatings were deposited by sequential exposure of the ZnO to nickelocene ($NiCp_2$) and O_3. The temperature of $NiCp_2$ precursor was maintained at 80 °C and the deposition was conducted with a substrate temperature of 150 °C. Finally, after the ALD process, the samples were transferred to a furnace and reduced at 450 °C in 5% H_2/Ar atmosphere for 2 h.

2.3 Sample characterization

X-ray diffraction (XRD) patterns were collected on a Bruker D8 Advance X-ray diffractometer using a Cu *Kα* source (λ = 0.154056 nm). Scanning electron microscopy (SEM) images were obtained using a HITACHI S-3000N microscope. Transmission electron microscopy (TEM) and high-resolution TEM (HRTEM) images were taken on a JEOL-2100 microscope instrument at an acceleration voltage of 200 kV. The composition and elemental maps of the samples were analyzed by energy-dispersive X-ray (EDX) spectroscopy using an EDX attachment to the SEM instrument. The specimens for measuring the EM properties were prepared by uniformly mixing 60 wt.% ZnO or ZnO@Ni with paraffin and pressing the mixture into a cylindrical shape. Then the cylinder was cut into a toroid of 7.00 mm outer diameter and 3.04 mm inner diameter for measurement. The relative permeability and permittivity values of the mixture were determined and obtained by measuring the *S*11 and *S*21 parameters between 2 and 18 GHz with an AV3629D network analyzer by using the transmission/reflection coaxial line method.

3. Results and discussion

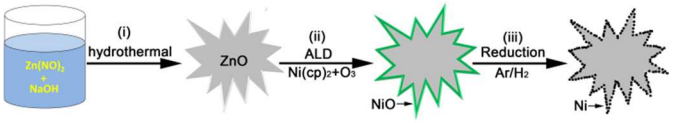

Fig. 1 Synthetic route for fabricating the ZnO@Ni core−shell composites.

The process for preparation of the ZnO@Ni core−shell composites can be divided into three steps as illustrated in Fig. 1. First, the flower-like ZnO was synthesized via a hydrothermal reaction at 160 °C. Second, the NiO-coated ZnO (ZnO@NiO) core−shell structures were obtained via an ALD approach using the as-prepared ZnO as the starting templates. Third, ZnO@Ni composites were obtained by annealing ZnO@NiO at 450 °C for 2 h under a mixture of H_2/Ar flow in a tube furnace.

XRD analysis was carried out to investigate the crystal phases of the as-synthesized products. Fig. 2 presents the XRD profiles of ZnO and ZnO@Ni (prepared by 800 cycles of NiO deposition, and then a hydrogen reduction) composites. For ZnO, all of the diffraction peaks can be indexed to those of hexagonal phase of zincite with the lattice parameters of a = 3.242 Å and c = 5.176 Å, which are consistent with the reported values (Joint Committee on Powder Diffraction Standards (JCPDS), powder diffraction file no. 01−1136). No clear diffraction peaks of NiO were found after 800 ALD cycles of NiO deposition (Fig. S1), which is probably due to the poor crystallinity and low content of NiO in the composites. After ZnO@Ni composites were formed by hydrogen reduction, two relatively weak peaks at 2θ = 44.5º and 51.8º are associated with the planes (111) and (200) of the face-centered cubic crystal structure of nickel phase (JCPDS card 87−0712), respectively. No peaks due to other undersigned phases are observed.

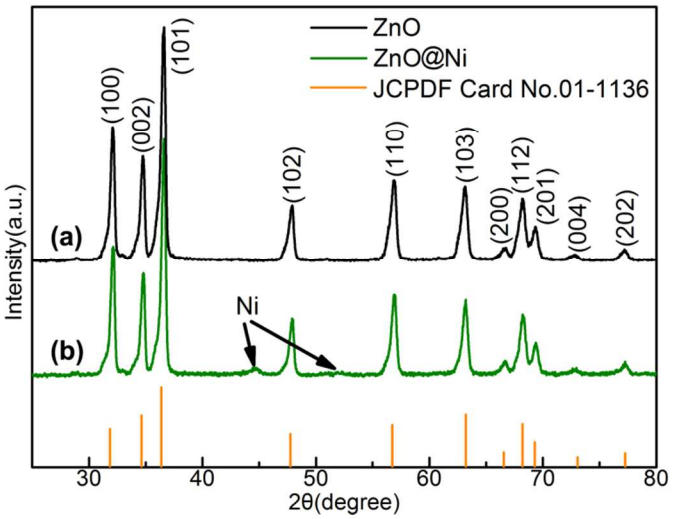

Fig. 2 XRD patterns of ZnO and ZnO@Ni composites.

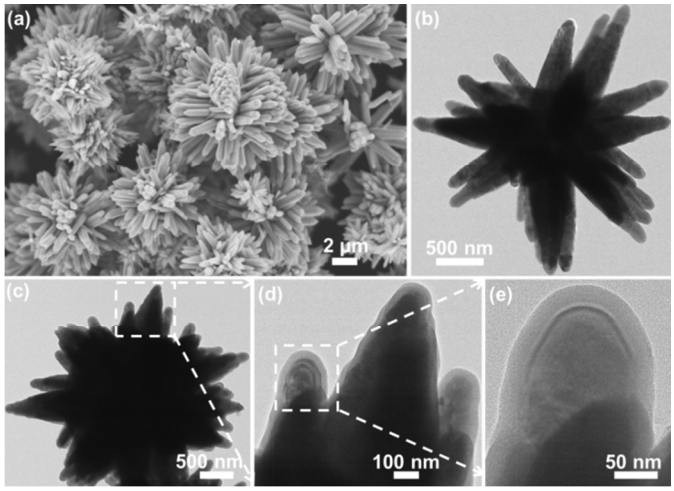

Fig. 3 (a) SEM and (b) TEM images of ZnO. (c−e) TEM images of ZnO@NiO obtained by applying 800 ALD cycles of NiO deposition.

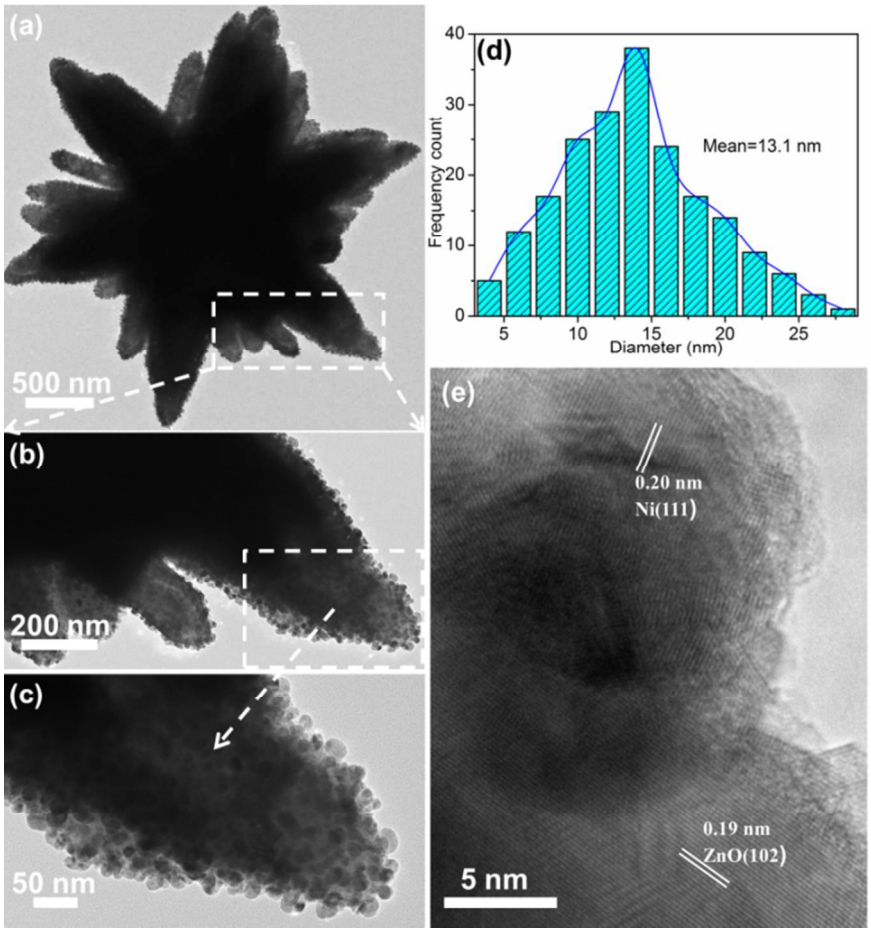

Fig. 4 (a–c) TEM images of ZnO@Ni. (d) The size distribution analysis of Ni nanoparticles. (e) HRTEM image of ZnO@Ni.

Fig. 3a and b display representative SEM and TEM images of the starting ZnO used in this study. It can be seen that ZnO presents a flower-like hierarchical structure assembled by the ZnO nanorods with diameter of 100–400 nm and length up to a few microns. Figs. 3c–e show TEM images of ZnO@NiO obtained by applying 800 ALD cycles of NiO deposition. The formed ZnO@NiO core−shell structures are clearly visible due to their different contrasts. The NiO shells are about 16 nm thick, which corresponds to a growth rate of about 0.2 Å per cycle. The HRTEM image (Fig. S2) shows no obvious lattice fringes, which indicates the poor crystallinity of as-deposited NiO. The elemental mapping results demonstrate the uniform distribution of NiO on the surface of flower like ZnO@NiO (Fig. S3).

Figs. 4a–c show low-resolution TEM images of the as-synthesized flower-like ZnO@Ni structure. It can be clearly seen that the surfaces of ZnO are densely covered by Ni nanoparticles with a narrow particle size distribution and an average size of 13.1 nm (Fig. 4d). The distribution of Ni nanoparticles on each ZnO nanorod is uniform, and no significant conglomeration of Ni nanoparticles or large vacancies on the surface of ZnO are observed. Several rings from selected area electron diffraction (SAED) pattern recorded on an individual ZnO@Ni nanorod can be assigned to diffraction planes of the cubic phase of Ni and the hexagonal phase of ZnO in agreement with the XRD data (Fig. S4). The HRTEM image highlights the well-defined crystalline lattice spacings of 0.19 and 0.20 nm, which can be indexed as (111)

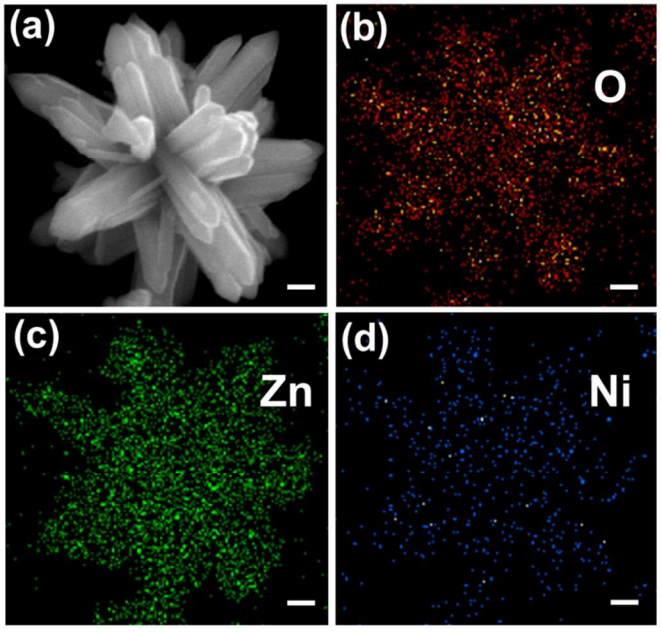

Fig. 5 (a) SEM of the ZnO@Ni and corresponding elemental mapping images of (b) O, (c) Zn and (d) Ni. Scale bar: 200 nm.

Table 1 Detailed comparison the value of minimum RL between ZnO and ZnO@Ni.

d (mm)	1.2	1.4	1.6	2.0	2.4
ZnO, RL_{min} (dB)	−1.4	−3.0	−5.8	−9.3	−10.8
ZnO@Ni, RL_{min} (dB)	−19.9	−37.6	−38.6	−48.0	−31.2

crystal planes of ZnO and (102) crystal planes of Ni (Fig. 4f), respectively. The elemental maps of Zn, O and Ni demonstrate that the Ni element is evenly distributed on the surface of ZnO and maintains a consistent flower-like morphology (Fig. 5).

Microwave absorption properties were investigated by mixing 60 wt.% the samples with paraffin. The reflection loss (RL) curves of ZnO-paraffin and ZnO@Ni-paraffin were derived from the relative complex permittivity and permeability at a given frequency and layer thickness according to the transmit line theory, which can be expressed as the following equations 1 and 2:[26,27]

$$Z_{in} = Z_0(\mu_r/\varepsilon_r)^{1/2}\tanh[j(2\pi fd/c)(\mu_r\varepsilon_r)^{1/2}] \quad (1)$$

$$\mathrm{RL} = 20\log\left|(Z_{in} - Z_0)/(Z_{in} + Z_0)\right| \quad (2)$$

where Z_{in} is the input impedance of the absorber, Z_0 the impedance of free space, μ_r the relative complex permeability, ε_r the complex permittivity, f the frequency of microwaves, d the thickness of the absorber, and c the velocity of light. A RL value of −10 dB is comparable to 90% microwave absorption. In general, materials with RL values of less than −10 dB absorption are considered as suitable EM wave absorbers.

Table 2 EM absorption properties of some recently reported ZnO-based additives

EM absorbing materials	RL_{min} (dB)	Thickness	Ref
netlike ZnO	−37.0	4.0 mm	19
ZnO	−21.9	3.0 mm	18
CNT/ZnOw	−37.0	3.0 mm	28
ZnO/$CoFe_2O_4$	−28.2	1.5 mm	20
Fe/ZnO	−33.5	5.0 mm	30
CNTs/T-ZnO/EP	−23.0	1.5 mm	29
ZnO@Ni	−48.0	2.0 mm	This work
ZnO@Ni	−27.3	1.5 mm	This work

It can be seen in Fig. 6a that the value of minimum RL of ZnO is −4.25 dB at 18 GHz with a thickness of 1.5 mm, while the ZnO@Ni shows a minimum RL value of −27.3 dB with the same thickness. The microwave absorption value less than –10 dB for ZnO@Ni is in the range of 12.1–17.4 GHz corresponding to a bandwidth of 5.3 GHz. Especially, a minimum RL value of −48.0 dB at 10.4 GHz is obtained from the ZnO@Ni core−shell structures with a thickness of 2 mm (Fig. 6b). To reveal in detail the influence of thickness on the

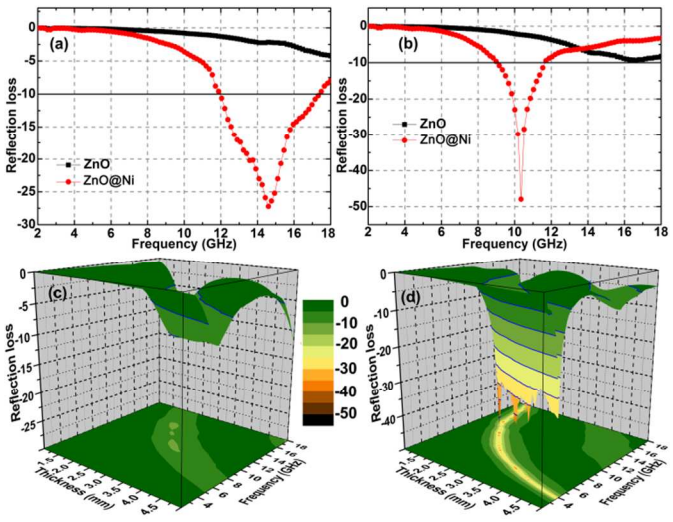

Fig. 6 RL curves of the product/paraffin composites with a thickness of (a) 1.5 mm and (b) 2 mm in the frequency range of 2–18 GHz. Three-dimensional representations of RL of (c) ZnO and (D) ZnO@Ni.

absorption properties, three-dimensional RL values of ZnO and ZnO@Ni are shown in Fig. 6c and d. The RL of ZnO can hardly reach −10 dB which means 90% microwave absorption in the range of 1.0−5.0 mm. For ZnO@Ni, the absorption band for RL values below −10 dB almost covers the whole frequency range, with the variation of thickness. Moreover, the absorption bandwidth for RL below −20 dB (99% absorption) also covers a wide frequency range (3.8–17.9 GHz) over the absorber thickness of 1.5–5 mm. The detailed comparison of EM absorption properties between ZnO and ZnO@Ni is shown in Table 1. Obviously, the ZnO@Ni exhibits substantially enhanced microwave absorption properties compared to ZnO. In addition, compared with other recently ZnO-based absorption materials,[18−20,28−30] the present ZnO@Ni not only has a strong absorption and a broad bandwidth but also small coating thickness, as shown in Table 2. Thus, the deposition of magnetic materials on the surface of ZnO is a very efficient way for the improvement of the EM absorption properties.

Dielectric loss and magnetic loss are well-known mechanisms normally responsible for energy attenuation in EM wave absorbers. Absorption capacity depends on the relative complex permittivity ($\varepsilon_r = \varepsilon' + i\varepsilon''$) and permeability ($\mu_r = \mu' + i\mu''$) of EM wave absorbers determined by their nature, size, and microstructure.[31,32] To uncover the possible absorption mechanism of the as-synthesized samples, the ε_r and μ_r of the

paraffin composites containing 60 wt.% of the samples were evaluated at 2–18 GHz. As shown in Fig. 7a, it can be seen that the ε' value of ZnO/paraffin composites is in the range of 5.8–7.4 and displays a slow decline in the frequency range of 2–18 GHz, while the ZnO@Ni/paraffin composites show much higher ε' value. The ε' value decreases gradually from 16.0 at 2.0 GHz to 11.7 at 10.2 GHz, then increases to 12.6 at 12.7 GHz, and decreases to at 11.6 at 18.0 GHz. The ε′ value of the ZnO@Ni is thus estimated to be about 2.2 times as that of the pure ZnO in the frequency range of 2–18 GHz. It can be seen in Fig. 7b that ZnO/paraffin composites show relatively constant ε'' value of 1.20–1.44, in the frequency range of 2–18 GHz, but ZnO@Ni/paraffin composites have much higher ε'' value in the same frequency range. The ε'' value is in the range of 3.8–5.3 and exhibits broad dual peaks at 10.0 and 13.9 GHz, respectively. As the paraffin has a very small ε'' value (near zero) at microwave frequency, thus ZnO@Ni has 3.2 times higher ε'' value as that of pure ZnO in the frequency range of 2–18 GHz.

It is known that, the ε' and ε'' of the complex permittivity represent the energy storage and dissipation capability, respectively. Thus the higher ε′ and ε'' values indicate that ZnO@Ni is much higher efficiency in storing and dissipating the electrical energy. Moreover, we calculated the dielectric loss tangents (tan $\delta_E = \varepsilon''/\varepsilon'$) of the ZnO and ZnO@Ni, in which the maximum values of tan δ_E are 0.24 and 0.39, respectively (Fig. 7c). The relatively high values of tan δ_E imply that the ZnO@Ni exhibits more intense dielectric loss. The Debye dipolar relaxation can be utilized to understand absorbing mechanisms of the dielectric loss materials. Four superimposed Cole−Cole semicircles (Fig. S5) are found for the ZnO@Ni samples, which may suggest that there are multiple dielectric relaxation processes. It also demonstrates that the depositing magnetic materials on the surface of ZnO can improve the intensity of the Debye dipolar relaxation process. Interfacial polarization occurs whenever there is a buildup of a charge at a boundary between two regions or materials.[33] In present work, benefiting from the highly controllable ALD technology, the uniform Ni NPs obtained after the reduction process were integrated firmly with the surface of ZnO. The charge transfer between ZnO and Ni also occurs with little hindrance. Therefore, the interfacial polarization and associated relaxation should contribute to the enhanced dielectric loss and microwave absorption performance.

The frequency dependence of the measured μ' and μ'' values of the complex permeability of ZnO and ZnO@Ni are shown in Fig. 8a and b. It can be seen that the μ' and μ'' values of ZnO are in the range of 0.98–1.18 and 0–0.1, respectively. For ZnO@Ni, the μ' and μ'' values show a slight increase in the frequency range of 2–18 GHz and are in the range of 1.02–1.31 and 0–0.18, respectively. The magnetic loss tangents (tan $\delta_M = \mu''/\mu'$) of the ZnO and ZnO@Ni have a same trend as μ'' (Fig. 8c), which suggests that the ZnO@Ni samples are more efficient in dissipating magnetic energy. Considering only 5.4 wt.% of Ni contained in ZnO@Ni composites (Fig. S6), application of ALD technology to deposit magnetic materials would be very promising to improve magnetic loss of microwave absorbers.

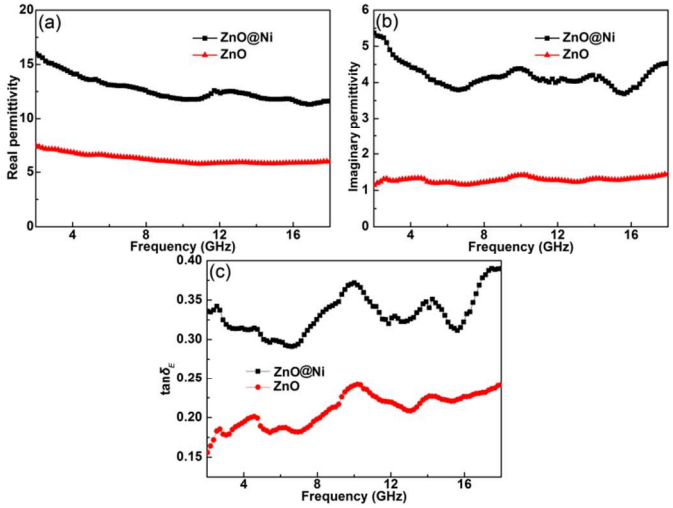

Fig. 7 The frequency dependence of (a) real permittivity, (b) imaginary permittivity and (c) dielectric loss tangents of ZnO-paraffin composite and ZnO@Ni-paraffin composite.

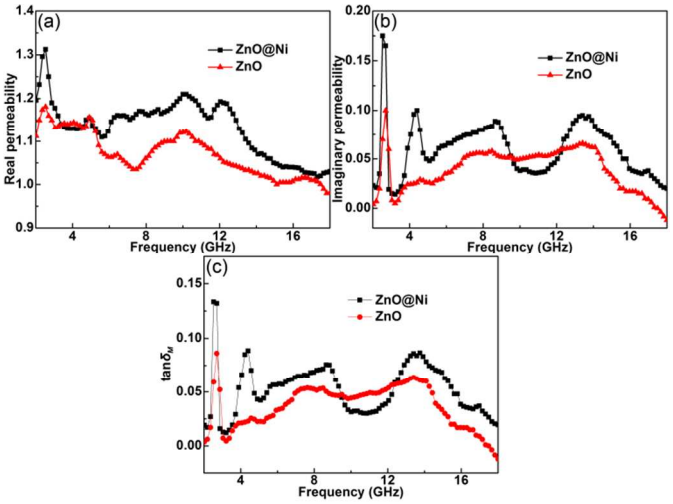

Fig. 8 The frequency dependence of (a) real permeability, (b) imaginary permeability and (c) magnetic loss tangents of ZnO-paraffin composite and ZnO@Ni-paraffin composite.

In the microwave frequency band, magnetic loss mainly comes from eddy current effects, natural resonance and exchange resonance. The eddy current loss contribution to the μ'' value is related to the thickness (d) and the electrical conductivity (σ) of materials, which can be expressed by the equation $\mu'' \approx 2\pi\mu_0(\mu')^2\sigma d^2 f/3$, where μ_0 is the permeability of vacuum. According to this equation, if the magnetic loss only originates from the eddy current loss, the values of $\mu''(\mu')^{-2}f^{-1}$ should be constant when the frequency is changed. As shown in Fig. 9, it can be seen that the values ($\mu''(\mu')^{-2}f^{-1}$) of ZnO@Ni show several obvious peaks, suggesting that eddy current loss is not the dominant magnetic loss. The natural resonance occurs usually at a lower frequency than the exchange resonance.

Therefore, it can be seen that the peak around 4.3 GHz is induced by the natural resonance, and the other two resonance peaks are induced by the exchange resonance.

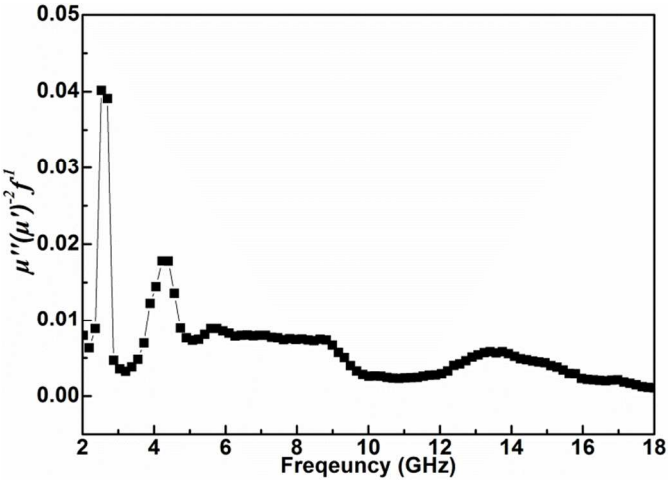

Fig. 9 Plot of $\mu''(\mu')^{-2}f^{-1}$ vs. frequency for ZnO@Ni composite.

In addition, EM wave attenuation in the interior of absorber is one of key factors for an excellent absorber. The attenuation constant α, which determines the attenuation properties of materials, can be denoted by[34,35]:

$$\alpha = \frac{\sqrt{2}\pi f}{c} \times \sqrt{(\mu''\varepsilon'' - \mu'\varepsilon') + \sqrt{(\mu''\varepsilon'' - \mu'\varepsilon')^2 + (\mu'\varepsilon'' + \mu''\varepsilon')^2}}$$

where f is the frequency of microwave and c is the velocity of light. Fig. 10 shows the dependence of the attenuation constant α in the frequency range of 2–18 GHz. It can be seen that the ZnO@Ni-paraffin composite has larger attenuation constant over the whole frequency range, which further confirms its excellent absorption.

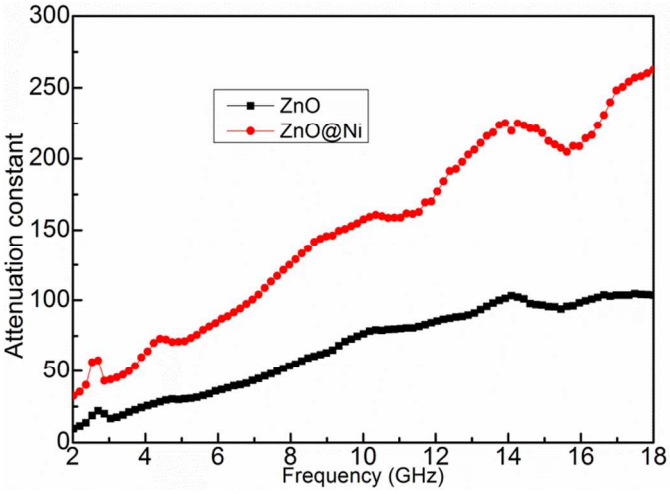

Fig.10 Attenuation constant of ZnO-paraffin composite and ZnO@Ni-paraffin composite.

Conclusions

In summary, an atomic layer deposition (ALD) method has been employed to synthesize Ni-coated ZnO nanohybrids. The as-prepared ZnO@Ni composites show superior EM wave absorbing characteristics compared with those of ZnO. The effective absorption bandwidth below –10 dB reaches 5.3 GHz for ZnO@Ni with a thickness of only 1.5 mm. Moreover, when the match thickness is 2.0 mm, the minimum RL is –48.0 dB at 10.4 GHz. The integration of multiple dielectric−magnetic loss intrigued by unique structure is responsible for excellent absorption ability of ZnO@Ni composites. Such results indicate that the present ZnO@Ni may be the attractive candidate material as a strong absorption, broad bandwidth, small coating thickness and low cost microwave absorber.

Acknowledgements

This work was supported by the National Natural Science Foundation of China (51362010), the Nature Science Foundation of Hainan Province (514207, 514212), the Scientific Research Projects of Colleges and Universities of Hainan Province (HNKY2014-14).

Notes and references

[a] Key Laboratory of Chinese Education Ministry for Tropical Biological Resources, Hainan University, Haikou, 570228, P. R. China
E-mail: wangengping001@163.com (G. P. Wan)
E-mail: lsw00@hotmail.com (S. W. Lin)
[b] State Key Laboratory of Coal Conversion, Institute of Coal Chemistry, Chinese Academy of Sciences, Taiyuan 030001, China
E-mail: qinyong@sxicc.ac.cn (Y. Qin)

Electronic Supplementary Information (ESI) available: XRD pattern of NiO@ZnO composites (Fig. S1); HRTEM image of NiO@ZnO (Fig. S2); SEM and elemental mapping images of ZnO@NiO (Fig. S3); SAED pattern of an individual ZnO@Ni nanorod (Fig. S4); Typical Cole–Cole semicircles (ε'' versus ε') for ZnO and ZnO@Ni composites (Fig. S5); EDS of ZnO@Ni (Fig .S6). See DOI: 10.1039/b000000x/

1 B. Wen, M. Cao, M. Lu, W. Cao, H. Shi, J. Liu, X. Wang, H. Jin, X. Fang, W. Wang and J. Yuan, *Adv. Mater.*, 2014, **26**, 3484.
2 G. Wang, Z. Gao, S. Tang, C. Chen, F. Duan, S. Zhao, S. Lin, Y. Feng, L. Zhou and Y. Qin, *ACS Nano*, 2012, **6**, 11009.
3 R. Che, L. M. Peng, X. F. Duan, Q. Chen and X. Liang, *Adv. Mater.*, 2004, **16**, 401.
4 G. Wang, Z. Gao, G. Wan, S. Lin, P. Yang and Y. Qin, *Nano Research*, 2014, **7**, 704.
5 L. Liu, M. Flores and N. Newman, *Phys. Rev. Lett.*, 2012, **109**, 257601.
6 F. Xia, J. Liu, D. Gu, P. Zhao, J. Zhang and R. Che, *Nanoscale*, 2011, **3**, 3860.
7 K. Lakshmi, H. John, K. Mathew, R. Joseph and K. George, *Acta Mater.*, 2009, **57**, 371.
8 E. Håkansson, A. Amiet and A. Kaynak. *Synth. Met.*, 2006, **156**, 917.
9 X. Zhang, P. Guan and X. Dong, *Appl. Phys. Lett.*, 2010, **97**, 033107.
10 C. Wang, X. Han, P. Xu, J. Wang, Y. Du, X. Wang, W. Qin and T. Zhang, *J. Phys. Chem. C*, 2010, **114**, 3196.
11 G. Sun, B. Dong, M. Cao, B. Wei and C. Hu, *Chem. Mater.*,

2011, **23**, 1587.
12 J. Liu, R. Che, H. Chen, F. Zhang, F. Xia, Q. Wu and M. Wang, *Small*, 2012, **8**, 1214.
13 N. N. Song, Y. J. Ke, H. T. Yang, H. Zhang, X. Q. Zhang, B. G. Shen and Z. H. Cheng, *Sci. Rep.*, 2013, **3**, 2291.
14 X. Y. Fang, M. S. Cao, X. L. Shi, Z. L. Hou, W. L. Song and J. Yuan, *J. Appl. Phys.*, 2010, **107**, 054304.
15 Q. Hu, G. Tong, W. Wu, F. Liu, H. Qian, D. Hong, *CrystEngComm*, 2013, **15**, 1314.
16 L. Kong, X. Yin, F. Ye, Q. Li, L. Zhang and L. Cheng, *J. Phys. Chem. C*, 2013, **117**, 2135.
17 R. Zhuo, H. Feng, J. Chen, D. Yan, J. Feng, H. Li, B. Geng, S. Cheng, X. Xu and P. Yan, *J. Phys. Chem. C*, 2008, **112**, 11767.
18 R. Zhuo, L. Qiao, H. Feng, J. Chen, D. Yan, Z. Wu and P. Yan, *J. Appl. Phys.*, 2008, **104**, 094101.
19 H. Li, Y. Huang, G. Sun, X. Yan, Y. Yang, J. Wang and Y. Zhang, *J. Phys. Chem. C*, 2010, **114**, 10088.
20 J. Cao, W. Fu, H. Yang, Q. Yu, Y. Zhang, S. Liu, P. Sun, X. Zhou, Y. Leng and S. Wang, *J. Phys. Chem. B*, 2009, **113**, 4642.
21 Y. J. Chen, G. Xiao, T. S. Wang, Q. Y. Ouyang, L. H. Qi, Y. Ma, P. Gao, C. L. Zhu, M. S. Cao and H. B. Jin, *J. Phys. Chem. C*, 2011, **115**, 13603.
22 X. Liu, D. Geng, H. Meng, P. Shang and Z. Zhang, *Appl. Phys. Lett.*, 2008, **92**, 173117.
23 X. Liu, B. Li, D. Geng, W. Cui, F. Yang, Z. Xie, D. Kang and Z. Zhang, *Carbon*, 2009, **47**, 470.
24 A. Ohlan, K. Singh, A. Chandra and S. K. Dhawan, *ACS Appl. Mat. Interfaces*, 2010, **2**, 927.
25 J. Zhu, S. Wei, N. Haldolaarachchige, D. P. Young and Z. Guo, *J. Phys. Chem. C*, 2011, **115**, 15304.
26 Y. Naito and K. Suetake, *IEEE Trans. Microwave Theory Tech.*, 1971, **19**, 65.
27 S. Kim, S. Jo, K. Gueon, K. Choi, J. Kim and K. Churn, *IEEE Trans. Magn.*, 1991, **27**, 5462.
28 G. Liu, L. Wang, G. Chen, S. Hua, C. Ge, H. Zhang and R. Wu, *J. Alloys Compd.*, 2012, **514**, 183.
29 H. Li, J. Wang, Y. Huang, X. Yan, J. Qi, J. Liu and Y. Zhang, *Mater. Sci. Eng. B*, 2010, **175**, 81.
30 X. Liu, D. Geng, P. Shang, H. Meng, F. Yang, B. Li, D. Kang and Z. Zhang, *J. Phys. D: Appl. Phys.*, 2008, **41**, 175006.
31 J. R. Liu, M. Itoh and K. I. Machida, *Appl. Phys. Lett.*, 2006, **88**, 062503.
32 X. Zhang, X. Dong, H. Huang, Y. Liu, W. Wang, X. Zhu, B. Lv, J. Lei and C. Lee, *Appl. Phys. Lett.*, 2006, **89**, 053115.
33 T. Xia, C. Zhang, N. A. Oyler and X. Chen, *Adv. Mater.*, 2013, **25**, 6905.
34 X. Liu, Z. Ou, D. Geng, Z. Han, J. Jiang, W. Liu and Z. Zhang, *Carbon*, 2010, **48**, 891.
35 J. Xiang, J. Li, X. Zhang, Q. Ye, J. Xu and X. Shen, *J. Mater. Chem.* A, 2014, **2**, 16905.

TOC

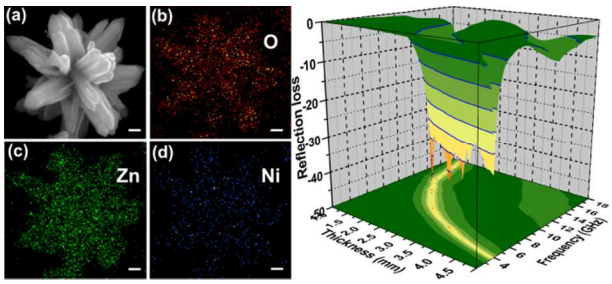

Ni-coated ZnO was fabricated by atomic layer deposition and exhibited remarkably improved microwave absorption properties compared to ZnO.